

Electromagnetic power induced from pair plasma falling into a rotating black hole II: An extensive WKB analysis in the slow rotation case

Yasufumi Kojima [★]

Department of Physics, Hiroshima University, Higashi-Hiroshima, Hiroshima 739-8526, Japan

16 June 2022

ABSTRACT

We examine Poynting flux generation due to pair plasma accreting onto a slowly rotating black hole. In particular, we consider the possibility of an outgoing flux at the horizon. Our approach is based on a two-fluid model representing a collisionless pair plasma. In the background, the plasma inflow is neutral and radial along the magnetic field lines of a split monopole in a Schwarzschild spacetime. A combined mechanism of dragging by the black hole’s spin and the Lorentz force produces charge separation and current flow, and hence electric and toroidal magnetic fields. By WKB analysis, two classes of solutions of perturbation equations for small black hole spin are identified: one is related to inward flux, and the amplitude inwardly increases; the other generates an outward flux with a peak position around $r = 3M$, tending to zero at the horizon. The power induced by the two-fluid effect is inversely proportional to plasma density, and is small in almost all astrophysical situations. A magnetic vacuum region is located elsewhere for effective Poynting flux generation.

1 INTRODUCTION

Blandford & Znajek (1977) (BZ) showed that there is an outgoing energy flux from a Kerr black hole. For the last four decades, the BZ model has been discussed as a promising mechanism to power relativistic jets in active galactic nuclei, micro quasars and gamma ray bursts. The mechanism can be roughly summarized as follows. A spinning black hole distorts the poloidal magnetic field \vec{B}_p and induces a poloidal electric field \vec{E}_p and a toroidal magnetic field \vec{B}_ϕ , which generate an outward Poynting flux $\vec{E}_p \times \vec{B}_\phi / (4\pi)$ along the magnetic field lines threading the spinning black hole. Thus, the rotation energy of the spinning black hole is electromagnetically extracted. The story is simple, but ambiguous in a sense. Total energy flux P through a radius in steady and axisymmetric electromagnetic field is expressed by integrating over a two-dimensional sphere: $4\pi P = -\int \Phi_{,\theta} S d\theta d\phi$, where Φ is an electric potential and S is a poloidal current function. The latter also describes B_ϕ , with some geometric functions (See, e.g., Thorne et al. 1986; Kojima 2015). This integral does not depend on the radius, when interaction between electromagnetic field and matter is completely neglected, like in force-free approximation. It merely represents conservation of electromagnetic energy flow. The mathematical expression represents the generation mechanism, but it should be note that not a dragging term $\vec{\beta}_\phi \times \vec{B}_p$, but a gradient term $\vec{\nabla}\Phi$ plays a crucial role, although stationary electric field generally consists of both terms. It is therefore necessary to understand how the potential Φ is determined as the origin of electromagnetic power.

To be more specific, we consider the problem in the ideal MHD approximation, which is good in many astrophysical cases. The electric potential Φ is constant along a poloidal magnetic line, which is characterized by a function G . Its derivative $\Omega_F \equiv d\Phi/dG$, which represents the angular velocity of the field line, is also constant along the line. In a steady problem, outward flux, say, at a certain radius far from a central object, leads to a horizon condition. Outgoing flux at the black hole horizon is mathematically shown to be possible only when Ω_F is in a certain range, which depends on the black hole spin. Consider a trivial example: when $\Omega_F = 0$ is fixed in the surroundings, the flux is zero because $\Omega_F = 0$ everywhere. Where and how is Ω_F determined? The issue is crucial for BZ process (See, e.g., Toma & Takahara 2014, 2016). On the analogy of a pulsar, the conversion of rotational energy to outward electromagnetic flux is sometimes discussed. Magnetic lines are anchored on the central neutron star, so that Ω_F is fixed at the stellar surface. The analogy is however inapplicable to the black

hole magnetosphere, since the black hole horizon is passive boundary. That is, the horizon condition is physically determined as a result of exterior behavior. There is then no good reason for any choice of Ω_F at the horizon (Punsly & Coroniti 1990).

Global steady-state force-free magnetospheres are modeled by numerically solving the relativistic Grad-Shafranov equation, in which there are singular surfaces and careful treatment is necessary. In this approach, Ω_F is mathematically specified to obtain a global solution (e.g., Uzdensky 2004, 2005; Tanabe & Nagataki 2008; Contopoulos et al. 2013; Nathanail & Contopoulos 2014; Pan & Yu 2015, 2016; Pan et al. 2017; Thoelecke et al. 2017). For example, the force-free solution is obtained by expansion with respect to the black hole spin. Split-monopole configuration is an exact solution in Schwarzschild spacetime, and Ω_F is zero. The first-order correction in Ω_F is uniquely determined to avoid the divergence which appears at the horizon in solving a second-order magnetic function. Similarly, Pan & Yu (2015, 2016) successfully calculated higher order corrections using the horizon regularity and convergence constrain in each order perturbation equation. The mathematical treatment is correct, but there might be no consensus as to whether or not the divergence is seriously taken. The force-free approximation breaks down near the horizon, since the mass inertia of plasma becomes important in that region. If so, the principle for determining Ω_F is questionable in astrophysical meanings. The extension to the MHD case is necessary. The formalism for stationary structure has already been given (e.g., Takahashi et al. 1990; Nitta et al. 1991; Beskin & Par'ev 1993), but it is quite difficult to obtain explicit solutions. The problem of Ω_F still remains, because of no successful works within the formalism. A time-dependent approach may be preferable to obtain the solutions. Actually, general relativistic magnetohydrodynamic simulations provide very interesting models (e.g., Koide et al. 2002; van Putten & Levinson 2003; Komissarov 2004, 2005; McKinney 2006; Komissarov & Barkov 2009; McKinney et al. 2012; Penna et al. 2013). Recently, very complicated but more realistic configurations with very intense magnetic fields have been successfully analyzed. The accretion inflow of matter, in disk flows called “magnetically arrested disks” (MADs) and jet launching in the vicinity of a central black hole have been explored simultaneously. However, it is hard to understand the origin of Ω_F from these remarkable numerical results.

As far as we consider the problem of Ω_F in a framework of MHD, the origin is likely to attribute to the boundaries. Otherwise, a model to fix Ω_F should be designed elsewhere in the interior. Here, we take a different approach to the origin of Ω_F (or Φ). We investigate whether or not there is an intrinsic mechanism in Kerr spacetime to produce it. If so, is the value at the horizon an appropriate one for the outward flux? For this purpose, we have to study plasma flows consistent with the electromagnetic fields in a two-fluid model (e.g., Kojima & Oogi 2009; Barkov et al. 2014; Petrova 2015, 2017), where Φ is no longer a constant along a magnetic field line. A previous paper (Kojima 2015, hereafter referred to Paper I) provided a general framework for an axially symmetric and stationary system around a Kerr black hole. It is difficult to consistently solve the whole set of equations, which is a coupled system of four partial differential equations. To obtain a definite solution, the effects of first-order slow spin were considered. Namely, in a Schwarzschild spacetime, the flow is radial along a split-monopole magnetic field. There is no charge density or current flow, and hence the electric and toroidal magnetic fields vanish everywhere. By taking into account the slow rotation, perturbations of these fields are induced. However, the analysis in Paper I is incomplete, since there is an error in eq. (42) of section 3.3. Here we correct that error and further study the electric-field generation problem in the slow rotation regime.

This paper is organized as follows. We first summarize our basic equations, which contain a large dimensionless parameter. These equations are not easy to solve numerically, so we approximate them by leading-order terms and discuss this limitation in section 2. Results based on WKB analysis are given in section 3. Finally, section 4 is our conclusion. We use units in which $c = G_N = 1$.

2 MODEL AND FORMULATION

2.1 Basic equations

A general formalism was given in Paper I for axisymmetric stationary states of two-component plasma flows consistent with electromagnetic fields in a Kerr spacetime. Perturbation equations with respect to the slow rotation of the black hole were also derived in order to evaluate the effect of the black hole spin. Here we also limit ourselves to the slow rotation regime and summarize the relevant equations below.

Schwarzschild spacetime with the first order rotational correction is given by

$$ds^2 = -\alpha^2 dt^2 + \alpha^{-2} dr^2 + r^2 d\theta^2 + r^2 \sin^2 \theta d\phi^2 - 2\omega r^2 \sin^2 \theta dt d\phi, \quad (1)$$

where

$$\alpha^2 = 1 - \frac{2M}{r}, \quad \omega = \frac{2M^2 a_*}{r^3}. \quad (2)$$

Here, M is a mass, and a_* is dimensionless small spin parameter.

Magnetic fields are assumed to be a split monopole with typical field strength B_0 and its perturbations, which are generally

described by two functions, $\delta G(r, \theta)$ and $\delta S(r, \theta)$:

$$[B_{\hat{r}}, B_{\hat{\theta}}, B_{\hat{\phi}}] = \left[\frac{B_0 M^2}{r^2} + \frac{\delta G_{,\theta}}{r^2 \sin \theta}, -\frac{\alpha \delta G_{,r}}{r \sin \theta}, \frac{\delta S}{\alpha r \sin \theta} \right]. \quad (3)$$

Electric fields are the first-order quantity described by a function $\delta \Phi(r, \theta)$:

$$[E_{\hat{r}}, E_{\hat{\theta}}, E_{\hat{\phi}}] = \left[-\delta \Phi_{,r}, -\frac{1}{\alpha r} (\delta \Phi_{,\theta} - \omega B_0 M^2 \sin \theta), 0 \right], \quad (4)$$

where the second term in $E_{\hat{\theta}}$ represents dragging a radial magnetic field in the azimuthal direction.

The plasma is modeled as a cold collisionless fluid of particles with mass m and electric charge $\pm e$. The flow of each component is described by the stream function $F_{\pm} = F_0 + \delta F_{\pm}$, where the background flow described by F_0 is radial along the magnetic monopole field. There is no net charge density or current flow in the background, to be consistent with the electromagnetic fields. The radial flow velocity is $v_{\hat{r}} = -(2/x)^{1/2}$, irrespective of species, and the common number density is $n_0 = \lambda n_c (2x^2(x-2))^{-1/2}$, where $x = r/M$, $n_c = B_0/(4\pi eM)$ and λ is a dimensionless number.

The perturbation δF_{\pm} is separated into two modes, ‘even’ $\delta F_+ = \delta F_-$ and ‘odd’ $\delta F_+ = -\delta F_-$. In the latter, a poloidal current and a toroidal magnetic field are induced since the current is produced by the difference between the two streams: $\delta S = 4\pi e(\delta F_+ - \delta F_-) \neq 0$. The flow directions in the meridian plane are opposite $\delta v_p^+ = -\delta v_p^-$, whereas those in the azimuthal direction are the same $\delta v_{\phi}^+ = \delta v_{\phi}^-$. The Lorentz forces for each component are opposite in the θ direction: $\pm e(\delta v_{\phi}^{\pm} B_{\hat{r}})$. The number densities do not balance, $\delta n_+ = -\delta n_-$, so that charge density $\delta \rho_e = e(\delta n_+ - \delta n_-) \neq 0$ is induced. The non-vanishing toroidal current is the second order $\delta j_{\phi} = e(\delta n_+ \delta v_{\phi}^+ - \delta n_- \delta v_{\phi}^-)$ in this mode. We restrict ourselves to odd mode perturbations $\delta F_+ = -\delta F_-$, and neglect the perturbation of the magnetic function δG in eq. (3).

Furthermore, the angular part is decoupled by the following forms:

$$\delta \Phi = B_0 M h(r) \cos \theta, \quad \delta F_{\pm} = \pm (\lambda n_c M^2 / 2) p(r) \sin^2 \theta, \quad \delta S = \lambda B_0 M p(r) \sin^2 \theta, \quad (5)$$

since the slow rotation corresponds to a dipole perturbation with spherical harmonic index $l = 1$. With these approximations, a system of four partial differential equations (Poisson’s equation, the Biot-Savart equation, and an equation for each stream function) is reduced to two pairs of ordinary differential equations for h and p ¹:

$$\left[\kappa^{-2} \frac{d^2}{dx^2} + U_0 - \kappa^{-2} U_2 \right] (xh) - \frac{\sqrt{2} k^{1/2}}{\kappa} \alpha^{-2} x^{-5/4} \left(x^{3/4} p \right) = \frac{4a_*}{\kappa^2 \alpha^2 x^4}, \quad (6)$$

$$\left[\kappa^{-2} \frac{d^2}{dx^2} - V_0 + \kappa^{-2} V_2 \right] \left(x^{3/4} p \right) - \frac{1}{k^{1/2} \kappa} \alpha^{-2} x^{-5/4} (xh) = \frac{2a_*}{k^{1/2} \kappa \alpha^2 x^{13/4}}, \quad (7)$$

where $x = r/M$, and the potential terms are divided into

$$U_0 = (1/\sqrt{2x}), U_2 = 2/(\alpha^2 x^2), \quad (8)$$

$$V_0 = \sqrt{2} x^{-3/2} \alpha^{-2} v, \quad v \equiv 1 - k^{-1} (2x)^{-3/2} \alpha^2, \quad V_2 = 3/(16x^2). \quad (9)$$

In eqs. (6) and (7), two parameters are involved². One is a dimensionless plasma frequency $\kappa^2 \equiv \omega_p^2 M^2 = 4\pi e^2 (\lambda n_c) M^2 / m$, where the typical number density is estimated with multiplicity λ and ‘Goldreich-Julian density’ $n_c \equiv B_0/(4\pi eM)$. In astrophysical situations, κ is very large, $\kappa \sim 10^{10}$. Another parameter k represents the ratio of the rest mass energy density of pairs to the electromagnetic energy density: $k = (m \lambda n_c) / (B_0^2 / 4\pi)$. When $k \gg 1$, hydrodynamical effects, such as pressure, are important and energy flow by matter dominates. In this case, our treatment is no longer valid. However, our concern is magnetically dominated flow, so we do not consider the large k case. The multiplicity λ is expressed as $\lambda = k^{1/2} \kappa$. The reasonable condition $\lambda > 1$ leads to $\kappa^{-2} < k$. We also consider a lower bound of k , and take $k_c \approx 2.3 \times 10^{-2}$ in order to simplify our argument. The number k_c will be derived in the next subsection, and hence the range of k is of order 10^{-2} - 10^0 , which covers the astrophysically interesting cases.

2.2 Further approximation and limitation

It is a natural approximation to neglect higher order terms, except the derivative terms, with κ^{-n} ($n \geq 2$) in eqs. (6) and (7), because $\kappa \gg 1$. The equations are then reduced to decoupled equations for h and p , and the solution can be easily obtained. Explicit forms will be given in the next section. Setting $\kappa^{-2} U_2 = 0$ in eq. (6), the solution h is oscillatory, since the potential U_0 is positive definite. Similarly, eq. (7) without the term $\kappa^{-2} V_2$ gives an exponential type solution for p , as long as V_0 is

¹ This set of equations is obtained from eqs. (41) and (42) in paper I, but there was a mistake in eq. (42). The errata for paper I are given in the Appendix.

² There are three parameters in a two-fluid model (e.g. Barkov et al. 2014), but one associated with relaxation time vanishes due to our collisionless approximation.

positive. The condition for this is given by $k > k_c \approx 2.3 \times 10^{-2}$. When $k < k_c$, the potential V_0 becomes negative in a range $r_1 < r < r_2$, and the function becomes oscillatory there. The whole solution is obtained by matching functions at r_1 and r_2 . We expect that such a solution is possible for only a particular value of k , namely, an eigenvalue, and requires more careful treatment. Our discussion is mainly limited to the range $k > k_c$.

Ignoring formally small terms proportional to κ^{-2} is a great simplification, but restricts the applicable range at the same time. The term $\kappa^{-2}U_2$ in eq. (6) increases toward the horizon because $U_2 \propto \alpha^{-2}$. The potential term $U_0 - \kappa^{-2}U_2$ becomes negative inside r_c , where a turning radius r_c is approximated as $1 - (2M/r_c) = \alpha^2(r_c) \approx \kappa^{-2} \ll 1$. The resulting solution changes from oscillatory to exponential growth/decay behavior across r_c . The term $\kappa^{-2}V_2$ in eq. (7) has a minor effect since it is small everywhere. Thus, we may safely ignore this term. The approximation to set $\kappa^{-2}U_2 = \kappa^{-2}V_2 = 0$ is limited to the range of $r > r_c (\approx 2M)$.

This limitation also affects the inner boundary condition. A regularity condition for eqs. (6) and (7) at the horizon is given by

$$k^{1/2}p + \frac{h}{\kappa} + \frac{a_*}{4\kappa} = 0. \quad (10)$$

Divergent terms in the limit of $\alpha \rightarrow 0$ are canceled in each equation, when eq. (10) is satisfied. This is nothing but the incoming wave condition of the electromagnetic fields, or the Znajek condition near the horizon $B_{\hat{\phi}} = -E_{\hat{\theta}}$ (Znajek 1978; Thorne et al. 1986). Equation (10) is derived in terms of the first-order perturbed functions h and p , from eqs. (3) and (4). The regularity condition is not the same in the approximated system with $\kappa^{-2}U_2 = 0$. Thus, the condition (10) is not necessary at the inner boundary $r \rightarrow 2M$, although r_c is numerically close to the horizon $2M$. The condition (10) is a passive one near the horizon, and is automatically satisfied in a regular system for $2M \leq r \leq r_c$.

3 WKB ANALYSIS

3.1 Solutions for homogeneous equations

We solve the homogeneous equations with the approximations $\kappa^{-2}U_2 = \kappa^{-2}V_2 = 0$ in eqs. (6) and (7). The solutions also describe the perturbations in a Schwarzschild black hole. We seek an approximate WKB solution of the form $p \propto \exp(\kappa W(x))$ and $h \propto \exp(\kappa W(x))$, where $\kappa (\gg 1)$ is a large number. Substituting these into eqs. (6)–(7), we find the leading-order solutions correct to order κ^{-1} . The four independent solutions (two pairs) given below are denoted by h_n^\pm and p_n^\pm .

A pair of type I solutions is given in terms of $x = r/M$ by

$$\begin{aligned} h_I^\pm &= x^{-1}U_0^{-1/4} \exp\left(\pm i\kappa \int^{r/M} U_0^{1/2} d\bar{x}\right) \\ &= 2^{1/8}x^{-7/8} \exp(\pm i\kappa_1 x^{3/4}), \end{aligned} \quad (11)$$

$$p_I^\pm = -2^{1/2}k^{-1/2}\kappa^{-1}x^{-1/2}Q^{-1}h_I^\pm, \quad (12)$$

where

$$Q = 1 - 2^{-1/2}k^{-1}\alpha^2x^{-5/2} \quad (13)$$

and $\kappa_1 = (2^{7/4}/3)\kappa$. The overall constant from the integral is adjusted to normalize the solution in eq. (11). This solution represents $p_I^\pm \ll h_I^\pm$ in the large κ limit: the larger function h_I^\pm is solely determined by eq. (6), and constrains the smaller p_I^\pm through eq. (7). The typical oscillatory scale is $\sim \kappa^{-1}M \sim \omega_p^{-1}$, and changes with the spatial distribution of the background number density.

Another pair of type II solutions is

$$p_{II}^\pm = x^{-3/4}V_0^{-1/4} \exp\left(\pm \kappa \int^{r/M} V_0^{1/2} d\bar{x}\right), \quad (14)$$

$$= 2^{-1/8}\alpha^{1/2}x^{-3/8}v^{-1/4} \exp(\pm g(x, \xi)), \quad (15)$$

$$h_{II}^\pm = 2k^{1/2}\kappa^{-1}x^{-1}Q^{-1}p_{II}^\pm, \quad (16)$$

where

$$g(x, \xi) = 2^{1/4}\kappa \int_\xi^x \alpha^{-1}\bar{x}^{-3/4}v^{1/2}d\bar{x}, \quad (17)$$

and ξ is a constant. This solution represents $h_{II}^\pm \ll p_{II}^\pm$ in the large κ limit. The larger p_{II}^\pm is solely determined by eq. (7), and constrains the smaller h_{II}^\pm through eq. (6). The situation is opposite to that of the type I solution. The two classes of solutions are clearly decoupled, since the coupling terms in eqs. (6) and (7) decrease with κ^{-1} . The electrostatic perturbation dominates in the type I solution, whereas the fluid perturbation dominates in the type II solution.

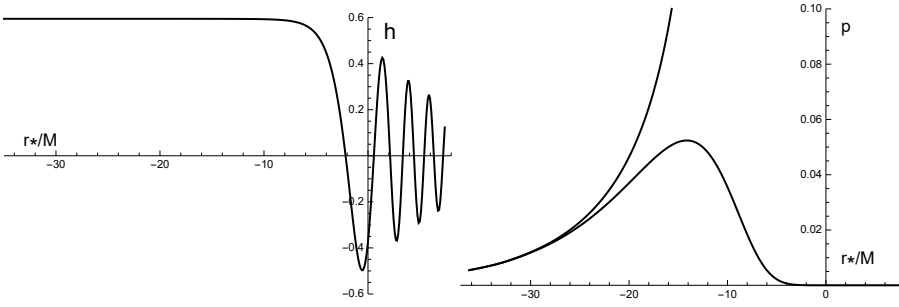


Figure 1. WKB solutions as a function of r_* . The type I solution h is shown in the left panel. Growing and decaying solutions p in the type II case are shown in the right panel. The parameters are chosen as $\kappa = 10$, $k = 0.1$. The valid range $r > r_c$ discussed in section 2.2 corresponds to $r_*/M > -7.2$ for $\kappa = 10$.

Figure 1 shows these functions with the tortoise coordinate $r_* \equiv r + 2M \ln(r/2M - 1)$. The two types are clearly distinguished by their functional behavior: one is oscillatory, and the other grows or decays exponentially. The function h_I in left panel of Fig. 1 is oscillatory outside a certain radius. The oscillation is determined by $\kappa_1 x^{3/4}$, and the wavelength becomes small with increasing κ ($\propto \kappa_1$). The oscillation is very rapid for a realistic value of κ . The envelope of the oscillations inwardly increase as $r^{-7/8}$, but the oscillation stops and the function tends to a constant as $r_* \rightarrow -\infty$. It is found that the transition point is very close to the critical radius r_c . Thus, asymptotic behavior for $r < r_c$ is meaningless, and the function there should be exponentially growing or decaying by the correction term $\kappa^{-2}U_2$ in eq. (6). The function p_{II} in the right panel of Fig. 1 tends to zero at the horizon with a factor $\alpha^{1/2}$, whereas it is exponentially growing or decaying for large r_* .

As shown in eqs. (12) and (16), the two functions h and p are connected by a function Q^{-1} in both type I and type II solutions. The function Q becomes zero, when $k < k_0 \approx 1.54 \times 10^{-2} (< k_c)$. There is a divergence at $Q = 0$, but this is an artifact of neglecting κ^{-2} terms. In our consideration limited to $k > k_c$, the function is approximated as $Q \approx 1$. Thus, we have $hp < 0$ in the type I solutions, whereas $hp > 0$ in the type II solutions. The relative sign is important for the direction of energy flow, as discussed in section 3.3.

3.2 Solutions with spacetime dragging effect

A general solution of eqs. (6) and (7) without the source terms is expressed by linear combinations of four functions as $h = \sum c_n^\pm h_n^\pm(x)$, and $p = \sum c_n^\pm p_n^\pm(x)$. The solution of the inhomogeneous equation is obtained by varying the coefficients c_n^\pm as $h = \sum c_n^\pm(x) h_n^\pm(x)$, and $p = \sum c_n^\pm(x) p_n^\pm(x)$. Putting these forms into eqs. (6) and (7), we have

$$\frac{1}{\kappa} \frac{dc_I^\pm}{dx} = \mp \frac{i}{2} \frac{J_I}{U_0^{1/4}} \exp \left[\mp i \kappa \int^{r/M} U_0^{1/2} dx' \right], \quad (18)$$

$$\frac{1}{\kappa} \frac{dc_{II}^\pm}{dx} = \pm \frac{1}{2} \frac{J_{II}}{V_0^{1/4}} \exp \left[\mp \kappa \int^{r/M} V_0^{1/2} dx' \right], \quad (19)$$

where

$$J_I = \frac{4a_*}{\kappa^2 \alpha^2 x^4} \left(1 - x^{-1/4} Q^{-1} \right), \quad (20)$$

$$J_{II} = \frac{2a_*}{k^{1/2} \kappa \alpha^2 x^{13/4}}. \quad (21)$$

Here we considered the leading order terms with respect to κ^{-n} . We integrate eq. (18) with boundary condition $c_I^\pm = 0$ at large radius. A particular solution of the inhomogeneous equation is given by

$$h_I^S = 2^{9/4} a_* \kappa^{-1} x^{-7/8} \int_x^{\text{out}} \left(1 - \xi^{-1/4} Q^{-1} \right) \alpha^{-2} \xi^{-31/8} \sin \left[\kappa_1 (\xi^{4/3} - x^{4/3}) \right] d\xi \quad (22)$$

and p_I^S can be obtained by the relation (12). Figure 2 shows the function $h_I^S \kappa / a_*$ in eq. (22) for $\kappa = 10^1, 10^2$ with $k = 0.1$. As $x = r/M$ decreases, h_I^S grows from zero and approaches a constant. The calculation is carried out for κ not too large, since the cost of the calculation increases with κ . However, a general property can be inferred: as κ increases, the growing point shifts to a smaller radius and the asymptotic constant of h_I^S is almost proportional to κ^{-1} . The highly oscillatory region contributes little to the integral (22) due to cancellation. The growth is thus related to the termination of the oscillation or a “frozen star” property near the black hole horizon. The growing point of h_I^S and the critical radius r_c are close to each other, and both move inward with increasing κ . The saturation region in Fig. 2 may be out of range, although the integral (22) is carried for small r to demonstrate the functional behavior. The solution h_I^S depends on the parameter k through Q , but this

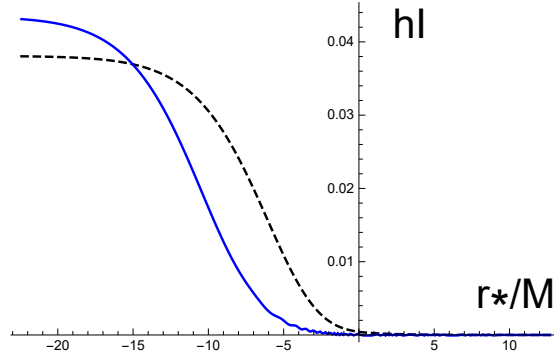


Figure 2. The special solution $h_{\text{I}}^{\text{S}}\kappa/a_*$ is displayed as a function of r_* . The solid line represents the function for $\kappa = 10^2$, whereas the dashed one is for $\kappa = 10^1$. The growth point shifts inward with the increase of κ . The result hardly depends on the parameter k , so long as $k > k_c$. Here $k = 0.1$ is used.

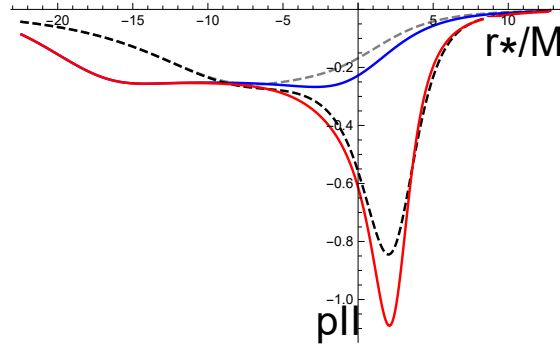


Figure 3. The special solution $p_{\text{II}}^{\text{S}}\kappa^{1/2}/a_*$ is displayed as a function of r_* . The solid lines represent the functions for $\kappa = 10^2$, whereas dashed ones are for $\kappa = 10^1$. The two lower curves with the minimum ~ -1 are for $k = 2.5 \times 10^{-2}$, whereas the upper ones are for $k = 0.1$.

dependence is weak since $Q \approx 1$. Thus, we estimate $h_{\text{I}}^{\text{S}} \propto \kappa^{-1}a_*$ and $p_{\text{I}}^{\text{S}} \propto k^{-1/2}\kappa^{-2}a_*$. These correspond to $E_p \propto \kappa^{-1}a_*$ and $B_\phi \propto \kappa^{-1}a_*$ in the electromagnetic perturbations.

We integrate eq. (19) with two boundary conditions: $c_{\text{II}}^+ = 0$ at a large radius, and $c_{\text{II}}^- = 0$ from an inner point. A particular solution of the inhomogeneous equation can be written in a concise form as

$$p_{\text{II}}^{\text{S}} = -\frac{a_*\alpha^{1/2}}{2^{1/4}k^{1/2}x^{3/8}v^{1/4}} \int_{\text{in}}^{\text{out}} \alpha^{-3/2}\xi^{-23/8}v^{-1/4} \exp[-|g(x,\xi)|] d\xi, \quad (23)$$

where $g(x,\xi)$ is defined in eq. (17). This is a method to solve inhomogeneous equations in terms of a Green function constructed by the WKB approximation. (see, e.g., [Bender & Orszag 1999](#)). The integral in eq. (23) provides a value of order κ^{-1} , so the normalized function $p_{\text{II}}^{\text{S}}\kappa^{1/2}/a_*$ is shown for $k = 0.1, 2.5 \times 10^{-2}$ and $\kappa = 10^1, 10^2$ in Fig.3. The function shows a steep minimum around $r_*/M \approx 2.5$, ($r/M \approx 3.3$) for $k = 2.5 \times 10^{-2}$. It becomes deeper as $k \rightarrow k_c$. This sharp minimum comes from the function v , which has a minimum at $x = r/M = 10/3$. The solutions are damped toward the horizon by a factor $\alpha^{1/2}$ in the homogeneous solutions p_{II}^{\pm} . Overall the functions scale as $p_{\text{II}}^{\text{S}} \propto k^{-1/2}\kappa^{-1}a_*$, and $h_{\text{I}}^{\text{S}} \propto \kappa^{-2}a_*$ through eq. (16), except for a region around the accidental point $r/M = 10/3$. These behaviors correspond to $E_p \propto \kappa^{-2}a_*$ and $B_\phi \propto \kappa^0a_*$ in the electromagnetic perturbations. In the limit of the ideal MHD case ($\kappa^{-1} \rightarrow 0$), a toroidal magnetic field is generated by dragging, whereas the electric potential remains zero as imposed in the outer boundary condition.

3.3 Electromagnetic energy flow

We now discuss the Poynting power induced by black hole spin. The electromagnetic energy flow originates from the product of the induced electric and toroidal magnetic fields. The energy through a sphere of radius r is calculated as (paper I):

$$P_{\text{em}}(r) = -\int (\sqrt{-g}T_{\text{em}}^r{}_{\text{t}}) d\theta d\phi = -\frac{1}{2} \int_{r=\text{const.}} (\delta\Phi_{,\theta} \delta S) d\theta. \quad (24)$$

Using the first-order perturbations, h and p in eq. (5), we have

$$P_{\text{em}} = \frac{2}{3}k^{1/2}\kappa hp(B_0M)^2. \quad (25)$$

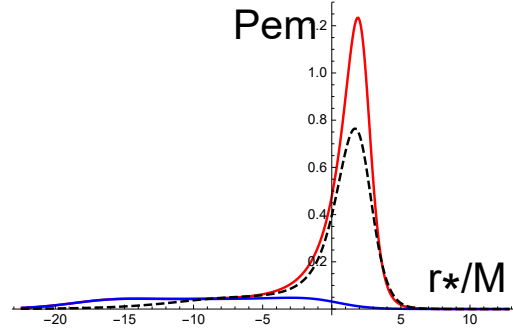


Figure 4. Outgoing Poynting flux $P_{\text{em}}\kappa^2/(a_*B_0M)^2$ as a function of r_* . The top solid line shows the result for the solution p_{II}^{S} and h_{II}^{S} with $k = 2.5 \times 10^{-2}$, $\kappa = 10^2$; the dashed line is for $k = 2.5 \times 10^{-2}$, $\kappa = 10^1$; and the lower flat line is for $k = 0.1$, $\kappa = 10^2$.

The sign of hp determines the direction of the energy flow. When $k > k_c$ h_{I}^{S} and p_{I}^{S} give $P_{\text{em}} < 0$, that is, inflow toward the black hole. There is a lower limit r_c , which is introduced due to our approximation of neglecting the higher order terms proportional to κ^{-2} . The interior solution in $2M < r < r_c$ is of the exponential type due to the negative potential ($U_0 - \kappa^{-2}U_2 < 0$ in eq. (6)), and can be obtained by matching interior and exterior solutions across r_c . We do not explicitly work out the full solution, but the sign of both functions h_{I}^{S} and p_{I}^{S} is likely to keep it in the exponential form inside r_c . Thus, the energy is still inflowing at the horizon.

When $k < k_0$, the function Q becomes negative between r_1 and r_2 , where the two radii are approximately given by $1 - (2M/r_1) \approx 2^3k \ll 1$ and $r_2/M \approx (2k^2)^{-1/5} \gg 1$. In this limited region, outgoing power is induced because $h_{\text{I}}^{\text{S}}p_{\text{I}}^{\text{S}} > 0$. Both r_c and r_1 are close to $2M$, but we have $r_c < r_1$ since $\kappa^{-2} \ll 1$ and $k \approx \mathcal{O}(1)$ in astrophysical situations. Therefore, the flux becomes negative again between r_c and r_1 , and the situation is the same near the horizon. Thus, the solutions h_{I}^{S} and p_{I}^{S} do not result in an outgoing flux at the horizon.

We next discuss a set of h_{II}^{S} and p_{II}^{S} , which satisfies $hp > 0$ when $k > k_c$. In this case an outgoing flux is generated. The function P_{em} is shown in Fig. 4. A sharp peak is located around $r_*/M \approx 2.5$ ($r/M \approx 3$), and P_{em} goes to zero on both sides ($r_*/M \rightarrow \pm\infty$). A Poynting flux is generated inside the peak. Namely, material energy is converted to electromagnetic energy in that region. Outside the peak, the conversion is in the opposite direction. The decrease of P_{em} at large r depends on the outer condition, $p_{\text{II}}^{\text{S}} \rightarrow 0$. The decrease of P_{em} toward the horizon comes from the functional behavior, $p_{\text{II}} \propto \alpha^{1/2}$, $h_{\text{II}} \propto \alpha^{1/2}$ as $\alpha \rightarrow 0$. The Poynting power is in order of magnitude $P_{\text{em}} \approx \kappa^{-2} \times P_{\text{BZ}}$, where $P_{\text{BZ}} (\approx (a_*B_0M)^2)$ is the Blandford and Znajek power. The magnitude of P_{em} is small due to a small factor κ^{-2} . The power can also be written as $P_{\text{em}} \propto n_0^{-1}B_0^2$, which decreases with number density n_0 .

3.4 Growth and decay of charge separation

In the previous subsection, the power is shown to be generated not around $r \approx 2M$ but around $r \approx 3M$. The generation mechanism fails toward the horizon. We study how and where a black hole spin affects neutral radial flow in background. Lorentz force, in particular, its θ -component is very important to produce non-radial spatial deviation:

$$\delta f_{\hat{\theta}}^{\pm} = \pm e(\delta E_{\hat{\theta}} + \delta v_{\hat{\phi}}^{\pm} B_{\hat{r}} - v_{\hat{r}} \delta B_{\hat{\phi}}) = \pm \frac{m\kappa^2}{Mk} \left[\frac{k^{1/2}}{\kappa\alpha x} \left(h + \frac{2a_*}{x^3} \right) - \frac{\alpha}{2x^3} p + \frac{2^{1/2}k}{\alpha x^{3/2}} p \right] \sin \theta, \quad (26)$$

where three terms in the first expression are explicitly written down by p and h in the second one³. We at first consider the behavior of $\delta f_{\hat{\theta}}^{\pm}$ in far region, where $r \gg 2M$ and $\alpha \approx 1$. The second term $\delta v_{\hat{\phi}}^{\pm} B_{\hat{r}}$ is dominant for type II solution ($h \ll p$), in a reasonable parameter range $\kappa^{-2} < k < 1$. Black hole drags the plasma in azimuthal direction irrespective of their electric charge ($\pm e$), and the Lorentz force acts in an opposite direction with respect to the fluid species. This mechanism causes spatial unbalance between two fluid components, and leads to nonzero charge density and current flows. Nonzero electric potential $\delta\Phi$ and toroidal magnetic field $\delta B_{\hat{\phi}}$ are thus produced. Toward black hole horizon ($\alpha \rightarrow 0$), third term increases due to a factor α^{-1} . This term has an opposite sign compared with the second one. Resultant toroidal magnetic field $\delta B_{\hat{\phi}}$ suppress growth of the θ -motion. As r further approaches the horizon, the force (26) seems to diverge. A relation between h and p in the coefficient of α^{-1} is nothing but the Znajek condition, eq.(10). So they should be canceled, and $\delta f_{\hat{\theta}}^{\pm}$ vanishes. The flow becomes radial near the horizon. The outward electromagnetic power also decreases there.

³ Equations (3),(4), $\delta v_{\hat{\phi}}^{\pm} = -k^{-1/2}\kappa p \sin \theta / (2\gamma_0 x)$ and $\alpha = \gamma_0^{-1}$ from eq.(38) in Paper I are used.

4 CONCLUSION

A poloidal electric field, in particular its potential part is essential to Poynting flux in a stationary and axially symmetric system. Once the potential is set to zero, for example, by a certain mechanism at an outer radius, the potential and resultant Poynting flux are both zero everywhere in a region threaded by magnetic field lines, since the potential is constant in the ideal MHD approximation. We have attempted to explore the origin of finite flux by a two-fluid effect, where the potential is no longer constant along the magnetic field.

There is a large dimensionless number contained in the formalism. That is, a ratio between microscopic scale of plasma and macroscopic scale of a black hole. This fact hinders the numerical integration for a realistic value. Using WKB analysis, we could classify modes and estimate the parameter dependence in a simple model. One mode describes an energy inflow toward the horizon, and the amplitude is finite there. The other describes an outgoing energy flow, and the luminosity has a sharp peak at some distance from the horizon. The magnitude decreases inward to zero, and the mode does not yield outgoing flow from the horizon. Furthermore, the resultant Poynting power is very small: it is reduced by a small factor κ^{-2} , where κ is a dimensionless plasma frequency, compared with the BZ power ($\approx (a_* B_0 M)^2$). With increasing κ , that is, increasing plasma number density, the ideal MHD condition becomes a better approximation, and the electric field vanishes to become consistent with the outer boundary value. The luminosity ($\propto n_0^{-1} B_0^2$) decreases with an increase of plasma density n_0 .

In this study, we found outward Poynting flux induced by the black hole spin, but failed to apply it in astrophysical situation. The two-fluid effect was not so important. However, this conclusion may be related to the simple model considered here. It is necessary to consider the effect on more elaborate models. The two-fluid effect is effective in a low-density region, so that a successful model requires such a magnetic vacuum region elsewhere in the black hole magnetosphere. The region is also related to a pair creation region or an origin of wind (e.g., Beskin & Kuznetsova 2000; Punsly 2008; Beskin 2010; Okamoto 2012, 2015). In their models, the position is proposed by some arguments. Another drawback in present model is the first-order limit of a Kerr black hole spin. The ergo-radius coincides with the horizon, so that there is no region inherent in the black hole spin. A rapidly rotating black hole significantly affects plasma flows and may produce an extremely low-density region, where the two-fluid effect is efficient. Further study is challenging.

APPENDIX:ERRATA IN PAPER I

There is a mistake in eq. (42) of paper I (Kojima 2015), which leads to an incorrect functional behavior for type II solutions. The coefficient $\alpha^{-2} s^{3/2}$ in front of dp/ds in eq. (42) should be changed to $s^{3/2}$. The factor α^{-2} leads to $p_{\text{II}}^{\pm} \propto \alpha$ and $h_{\text{II}}^{\pm} \propto \alpha^{-1}$ in paper I, but the correct behaviors are $p_{\text{II}}^{\pm} \propto \alpha^{1/2}$ and $h_{\text{II}}^{\pm} \propto \alpha^{1/2}$. See eqs. (14)–(16) in this paper. The special solution p_{II}^{S} (eq. (53) of paper I) is also wrong, and is corrected as eq. (23) in this paper. All figures with p_{II}^{S} or h_{II}^{S} in paper I are wrong.

ACKNOWLEDGEMENTS

This work was supported by JSPS KAKENHI Grant Number JP26400276.

REFERENCES

- Barkov M., Komissarov S. S., Korolev V., Zankovich A., 2014, *MNRAS*, **438**, 704
 Bender C. M., Orszag S. A., 1999, *Advanced mathematical methods for scientists and engineers I: asymptotic methods and perturbation theory*.
 Beskin V. S., 2010, *Physics Uspekhi*, **53**, 1199
 Beskin V. S., Kuznetsova I. V., 2000, *Nuovo Cimento B Serie*, **115**, 795
 Beskin V. S., Par'ev V. I., 1993, *Physics Uspekhi*, **36**, 529
 Blandford R. D., Znajek R. L., 1977, *MNRAS*, **179**, 433
 Contopoulos I., Kazanas D., Papadopoulos D. B., 2013, *ApJ*, **765**, 113
 Koide S., Shibata K., Kudoh T., Meier D. L., 2002, *Science*, **295**, 1688
 Kojima Y., 2015, *MNRAS*, **454**, 3902
 Kojima Y., Oogi J., 2009, *MNRAS*, **398**, 271
 Komissarov S. S., 2004, *MNRAS*, **350**, 1431
 Komissarov S. S., 2005, *MNRAS*, **359**, 801
 Komissarov S. S., Barkov M. V., 2009, *MNRAS*, **397**, 1153
 McKinney J. C., 2006, *MNRAS*, **368**, 1561
 McKinney J. C., Tchekhovskoy A., Blandford R. D., 2012, *MNRAS*, **423**, 3083
 Nathanail A., Contopoulos I., 2014, *ApJ*, **788**, 186
 Nitta S.-Y., Takahashi M., Tomimatsu A., 1991, *Phys. Rev. D*, **44**, 2295
 Okamoto I., 2012, *PASJ*, **64**, 50
 Okamoto I., 2015, *PASJ*, **67**, 89

- Pan Z., Yu C., 2015, [Phys. Rev. D](#), **91**, 064067
- Pan Z., Yu C., 2016, [ApJ](#), **816**, 77
- Pan Z., Yu C., Huang L., 2017, [ApJ](#), **836**, 193
- Penna R. F., Narayan R., Sądowski A., 2013, [MNRAS](#), **436**, 3741
- Petrova S. A., 2015, [MNRAS](#), **446**, 2243
- Petrova S. A., 2017, [J. Cosmology Astropart. Phys.](#), **5**, 041
- Punsly B., ed. 2008, Black Hole Gravitohydromagnetics Astrophysics and Space Science Library Vol. 355
- Punsly B., Coroniti F. V., 1990, [ApJ](#), **350**, 518
- Takahashi M., Nitta S., Tatematsu Y., Tomimatsu A., 1990, [ApJ](#), **363**, 206
- Tanabe K., Nagataki S., 2008, [Phys. Rev. D](#), **78**, 024004
- Thoelecke K., Tsuruta S., Takahashi M., 2017, [Phys. Rev. D](#), **95**, 063008
- Thorne K. S., Price R. H., MacDonald D. A., 1986, Black holes: The membrane paradigm
- Toma K., Takahara F., 2014, [MNRAS](#), **442**, 2855
- Toma K., Takahara F., 2016, [Progress of Theoretical and Experimental Physics](#), **2016**, 063E01
- Uzdensky D. A., 2004, [ApJ](#), **603**, 652
- Uzdensky D. A., 2005, [ApJ](#), **620**, 889
- Znajek R. L., 1978, [MNRAS](#), **185**, 833
- van Putten M. H. P. M., Levinson A., 2003, [ApJ](#), **584**, 937